Agonist-Induced Conformational Changes in Thyrotropin-Releasing Hormone Receptor Type I: Disulfide Cross-Linking and Molecular Modeling Approaches

Wei Huang,[‡,§] Roman Osman,[||] and Marvin C. Gershengorn*[,‡]

Clinical Endocrinology Branch, National Institute of Diabetes and Digestive and Kidney Diseases, National Institutes of Health, 50 South Drive, Building 50/4134, Bethesda, Maryland 20892, Graduate Program in Physiology, Biophysics and Molecular Medicine, Weill Graduate School of Medical Sciences of Cornell University, 1300 York Avenue, New York, New York 10021, and Department of Physiology and Biophysics, Mount Sinai School of Medicine, One Gustave L. Levy Place, New York, New York 10029

Received June 8, 2004; Revised Manuscript Received September 23, 2004

ABSTRACT: The conformational changes at the cytoplasmic ends of transmembrane helices 5 and 6 (TMH5 and TMH6) of thyrotropin-releasing hormone (TRH) receptor type I (TRH−R1) during activation were analyzed by cysteine-scanning mutagenesis followed by disulfide cross-linking and molecular modeling. Sixteen double cysteine mutants were constructed by substitution of one residue at the cytoplasmic end of TMH5 and the other at that of TMH6. The cross-linking experiments indicate that four mutants, Q263C/G212C, Q263C/Y211C, T265C/G212C, and T265C/Y211C, exhibited disulfide bond formation that was sensitive to TRH occupancy. We refined our previous TRH−R1 models by embedding them into a hydrated explicit lipid bilayer. Molecular dynamics simulations of the models, as well as *in silico* double cysteine models, generated trajectories that were in agreement with experimental results. Our findings suggest that TRH binding induces a separation of the cytoplasmic ends of TMH5 and TMH6 and a rotation of TMH6. These changes likely increase the surface accessible area at the juxtamembrane region of intracellular loop 3 that could promote interactions between G proteins and key residues within the receptor.

Seven transmembrane-spanning receptors (7TMRs)[1] constitute the largest membrane protein family in mammalian genomes that transduce extracellular signals to cytoplasmic signaling machineries. All 7TMRs appear to share a similar topological structure. In 2000, the first three-dimensional (3D) structure of a 7TMR, that of the inactive state of rhodopsin, was solved (*1*). However, the molecular details of rhodopsin conformation during light activation have not been delineated. Moreover, the structural changes upon agonist-induced activation of other 7TMRs are poorly defined.

Several biochemical and biophysical approaches have been used to attempt to understand the molecular mechanism of activation of 7TMRs. These include electron paramagnetic resonance (EPR) spectroscopy (*2*−*4*), cysteine scanning mutagenesis and disulfide cross-linking (*5*−*8*), construction of bis-his Zinc(II) binding sites (*9*−*11*), substituted cysteine accessibility (*12*), and fluorescence spectroscopy (*13*−*15*). Since different approaches address different structural and dynamic aspects, it is difficult to compare the conclusions from these studies directly. Except for rhodopsin, there are few 7TMRs that have been investigated with more than one approach.

One of the key questions for 7TMR function is how the interaction between the agonist and the 7TMR causes activation. It is a general assumption that agonist-induced transmembrane helix movement alters the conformation of the cytoplasmic surface of the receptor that interacts with G-protein. A number of studies support a key role of the domain including intracellular loop 3 (ICL3) in coupling to G proteins (*16*−*28*). In particular, residues within the amino- and carboxyl-termini of the ICL3 loops play important roles. However, a consensus recognition motif for G protein coupling has not been identified. In fact, ICL3 is one of the least conserved regions in 7TMRs.

The sequence Arg-Lys/Arg-Gln in the ICL3-TMH6 region is conserved among TRH−Rs from all species. These residues correspond to positions-261, 262, and 263 in mouse TRH−R1. It has been shown that in TRH−R1, substitution of both Arg-261 and Lys-262 by Gln led to mutant receptors that exhibited decreased TRH-stimulated signaling activities due to decreased coupling to Gq (*22*). Residues 218−225 in the TMH5−ICL3 region have also been shown to be involved in Gq coupling (*22, 29*). Therefore, the relative position of the cytoplasmic ends of TMH5 and TMH6 would likely influence optimal Gq coupling by affecting the

* To whom correspondence and reprint requests should be addressed. Mailing address: Marvin C. Gershengorn, Scientific Director, NIDDK, National Institutes of Health, 9000 Rockville Pike, Bethesda, MD 20892-1818. Tel: 301-496-4128. Fax: 301-496-9943. E-mail: marving@intra.niddk.nih.gov.

‡ National Institutes of Health.

§ Weill Graduate School of Medical Sciences of Cornell University.

|| Mount Sinai School of Medicine.

[1] Abbreviations: TRH, thyrotropin-releasing hormone; TRH−R, thyrotropin-releasing hormone receptor; 7TMR, seven transmembrane-spanning receptor; TMH, transmembrane helix; ECL, extracellular loop; ICL, intracellular loop; NEM, *N*-ethylmaleimide; CNBR, cyanogen bromide; EDTA, ethylenediaminetetraacetic acid; EGTA, ethyleneglycoltetraacetic acid; ATP, adenosine 5′-triphosphate; *β*-ME, *β*-mercaptoethanol; DM, *n*-dodecyl-*β*-maltoside; SDS−PAGE, sodium dodecyl sulfate polyacrylamide gel electrophoresis; DMPC, dimyristoylphosphatidylcholine; RT, room temperature.

10.1021/bi048808+ CCC: $30.25
Published on Web 01/20/2005

conformation of residues 261and 262, and residues from 218 to 225. In fact, using molecular modeling of several constitutively active mutants, we previously proposed a model in which activation of TRH−R1 releases constraints between TMH5 and TMH6 that increases the distances between the cytoplasmic ends of TMH5 and TMH6, and leads to Gq activation (*30*).

In this report, we attempt to gain further insight into the molecular mechanism of TRH−R1 activation induced by its natural agonist, thyrotropin-releasing hormone (TRH). We specifically studied the conformational changes at the cytoplasmic ends of TMH5 and TMH6. Since models are helpful to better understand and interpret experimental results, and could provide further testable hypotheses (*31*), we used a combination of experimental and modeling approaches. In our experiments, we used cysteine-scanning mutagenesis followed by disulfide cross-linking (*32*−*34*) to monitor conformational changes.

EXPERIMENTAL PROCEDURES

Materials. [^{3}H][methyl-His]TRH ([^{3}H]MeTRH) was purchased from NEN Life Science Products (Boston, MA). Restriction endonucleases, Vent DNA polymerase and deoxynucleotides were obtained from New England Biolabs, Inc. (Beverly, MA). Cell culture media, sera and oligonucleotides were from Gibco/Life Technology (Grand Island, NY). Bovine factor Xa and *N*-ethylmaleimide (NEM) were from Pierce Endogen (Rockford, IL). n-Dodecyl-β-maltoside was from Anatrace (Maumee, OH). 1D4 antibody was supplied by the National Cell Culture Center (Mineapolis, MN). Horseradish peroxidase-conjugated goat anti-mouse antibody, anti-biotin antibody and biotinylated protein markers were from Cell Signaling Technology (St. Louis, MO). Enhanced chemiluminescence Western blotting detection reagents and CNBR-activated sepharose were from Amersham Pharmacia Biotech (England). Complete EDTA-free protease inhibitor cocktail tablets were from Roche Diagnostics (Mannheim, Germany). The mammalian expression vector pcDNA3.1-(+) was from Invitrogen (Carlsbad, CA). Plasmids for reporter gene assays, pFR−Luc and pFA2-CREB (PathDetect In Vivo Signal Transduction Pathway *trans*-Reporting System) and QuikChange site-directed mutagenesis kit were from Stratagene (La Jolla, CA). DNA purification reagents were from Qiagen (Hilden, Germany). TRH, Luciferin, and other chemicals were from Sigma (St. Louis, MO). All reagents were analytical grade. C9 peptide (NH2-TETSQVAPA-COOH) was synthesized and verified using mass spectrometry. DNA sequencing was performed by Cornell BioResourceCenter.

DNA Constructs. The cDNA encoding mouse TRH−R1 was in the mammalian cell expression vector pcDNA3.1-(+). C9i3X-7C was constructed in four steps. 1) The C9 sequence with a diglycine linker (NH2-GGTETSQVAPA-COOH) was inserted into the C-terminus of mTRH−R1. The original residues 384−393, including Cys-388, were removed. Cys-335/337 were mutated to Gly by a single step PCR using pCDM8mTRH−R1−C335/337G (*35*) as the template, and subcloned into pcDNA3.1(+) using *Eco*R1 and *Not*I sites. 2) Two factor Xa sites (IDGRIEGR) were inserted in tandem between Ala-249 and Thr-250 of ICL3 of the previous construct. 3) The two cysteines on ICL2 (Cys-128/137) were substituted with Ala. 4) The endogenous cysteine on ICL3 (Cys-253) was substituted with Ser. These constructs were made by overlap PCR utilizing *Eco*R1 and *Not*I sites. C9i3X-7C has seven free endogenous cysteines, all of which are in the transmembrane helices (TMHs). Substitution of Cys-100 and Cys-157 (Cys-100/157) of C9i3X-7C to Ala resulted in a mutant referred to as C1. C4 was from substitution of Cys-36 and Cys-157 (Cys-36/157) of C9i3X-7C to Ala. C8 was from substitution of Cys-36/100 of C9i3X-7C to Ala. C9i3X-3C was from substitution of Cys-62/114/305/308 of C9i3X-7C to Ala. Sixteen double-cysteine mutants were from substitution of two residues of C9i3X-3C to Cys. Each double-cysteine mutant was from substitutions of one residue out of Leu-210-Phe-213 (TMH5) and the other out of Gln-263-Lys-266 (TMH6). These mutants were made using QuikChange site-directed mutagenesis kit. All constructs were verified by DNA sequencing.

Cell Culture and Transfection. HEK 293 EM cells (*36*) were grown in DMEM containing 10% fetal bovine serum. For receptor binding and reporter gene assays, cells were seeded in 24-well cell culture plates (60,000 cells/well) on the day before transfection. For Western blotting and disulfide cross-linking assay, cells were seeded in 10-cm cell culture dishes at 5×10^5 cells/dish 2 days before transfection. Cells were transfected with calcium phosphate. For reporter gene assays, transfection was with 1 μg/mL of plasmid DNA encoding the desired TRH−R1 gene, 1 μg/mL pFR−Luc and 1 μg/mL pFA2-CREB. For other experiments, transfection was with 1 μg/mL of receptor plasmid alone. Binding and reporter gene assays were performed after 24 h and the other experiments after 48 h.

Receptor Binding Assay. Binding experiments were carried out in buffer with cells in monolayer for 1 h at 37 °C as described (*37*). The concentrations of [^{3}H]MeTRH were 0.1−10 nM for saturation binding or 2 nM for competition binding. Inhibitory constants (K_i) for TRH were derived from competition binding experiments using the formula $K_i = (IC_{50})/(1 + ([L]/K_d))$, where IC_{50} is the concentration of unlabeled TRH that half-displaces specifically bound [^{3}H]MeTRH and K_d is the equilibrium dissociation constant for [^{3}H]MeTRH. K_ds were obtained by saturation binding. Curves were fitted by nonlinear regression analysis and drawn with the PRISM program (GraphPad Inc.).

Reporter Gene Assay. Cells in 24-well plates were transfected and after 6 h fresh media with 1% serum was added. After an additional 18 h, cells were washed with PBS and lysed with 0.5 mL of lysis buffer (25 mM GlyGly, pH 7.8; 15 mM $MgSO_4 \cdot 6H_2O$; 4 mM EGTA; 1 mM dithiothreitol; 1% Triton X-100). Cell lysates (0.025 mL) were combined automatically with 0.125 mL reaction buffer (25 mM GlyGly, pH 7.8; 15 mM $MgSO_4 \cdot 6H_2O$; 4 mM EGTA; 1 mM dithiothreitol; 15 mM KH_2PO_4; 2 mM ATP) and 0.025 mL luciferin (0.4 mM) in reaction buffer and the luminescence was measured for 10 s in a TR717 Microplate Luminometer (Tropix, Bedford, MA).

Cell Lysis. Cells were washed with ice-cold PBS buffer 48 h after transfection. One milliter of lysis buffer (1% n-dodecyl-β-maltoside (DM) in 50 mM Tris-Cl, pH 8.0 with 100 mM $(NH_4)_2SO_4$, 10% glycerol (v/v) and Complete© EDTA-free protease inhibitor cocktail tablets (1 tab/25 mL)) was added per 10-cm dish. The cells were removed using a cell scraper, transferred to eppendorf tubes, and incubated

for 30 min on an end-over-end rocker at 4 °C. The lysate was then spun at 15,000Xg to remove insoluble debris. In the experiments with TRH-occupied receptors, cells were rinsed once with ice-cold PBS. PBS containing 100 μM TRH was added to 10 cm dishes (5 mL per dish), and incubated for 4 h at 4 °C, and then lysed as above. In these lysates, 100 μM TRH was also added to lysis buffer.

Disulfide Cross-Linking with Cu-Phenanthroline. One milliliter of freshly prepared cell lysate was brought to room temperature and mixed immediately with 10 μL of a fresh preparation of Cu(II)-1,10-phenanthroline (5 mM $CuSO_4$ and 15 mM phenanthroline). The reaction was carried out at room temperature for 30 min (or indicated otherwise). The mixture was then mixed with 40 μL of stop reagent (freshly prepared 250 mM EDTA/250 mM NEM), and kept on ice for 1 h before immunoprecipitation.

Immunoprecipitation and Elution. 1D4 antibody was coupled to CNBR-activated sepharose at ~1 mg/mL. One milliter of freshly prepared cell lysate or cell lysate treated with Cu-phenanthroline was mixed with 5 μL of 1D4-beads and incubated overnight at 4 °C on an end-over-end rocker. After removing the supernatant, the beads were washed once with buffer A (0.1% DM in 50 mM Tris, pH 8.0 containing 100 mM NaCl pH 8.0) and twice with buffer B (0.1% DM in contained 50 mM Tris, pH 8.0 containing 100 mM NaCl and 6 mM $CaCl_2$). Buffer B was the factor Xa reaction buffer plus detergent (0.1% DM). The samples were kept at 4 °C throughout the steps. The beads were then carefully removed from wash buffer and mixed with 30 μL of elution buffer (250 μM C9 peptide in buffer B). After incubation for 2 h at RT, the eluate was separated from 1D4-beads. All the contaminants (protease inhibitors, Cu-phenanthroline, NEM and EDTA) that would interfere with factor Xa digestion were removed during this process.

Factor Xa Digestion. The eluted samples (30 μL /10-cm dish) were incubated with 1 μL of factor Xa at RT for 4 h. Each sample was divided into two aliquots. The reactions were terminated by adding 1/4 volume of 5-fold Laemmli sample buffer. One aliquot contained extra 1% of β-ME in the final mixture. The samples were heated for 1 h at 50 °C before loading to SDS−PAGE gel.

Western Blotting. Equal volumes of two aliquots of the same sample were loaded onto 8−16% Precast gels (Bio-Rad) with Prestained (precision, Bio-Rad) or biotinylated protein markers (Cell Signaling). After electrophoresis, proteins were electroblotted onto nitrocellulose membrane (0.2 μm) (Bio-Rad) by running at 20 V overnight in the Bio-Rad transferring buffer at 4 °C. Subsequent steps were performed at RT. Membranes were blocked with blocking buffer (10% nonfat dry milk in PBS containing 0.1% tween-20) for 1 h. Membranes were rinsed once with PBS/0.1% tween-20 (PBST), and incubated with primary antibody (1D4 antibody, 1 μg/mL in blocking buffer) for 1 h. After three washes with PBST, membranes were probed with horseradish peroxidase-conjugated secondary antibodies (goat anti-mouse IgG (1:3000) and goat anti-biotin IgG (1:1500) in PBST) for 40 min. After stringent washes of the membrane with PBST, antibody-associated proteins were visualized using an enhanced chemiluminescence detection kit. The signals were detected using KODAK BioMax-ML films.

Quantification of Western Blots. The films were digitized and the bands were quantified using a Bio-RAD fluoS multiimager and Quantity One software version 4.2.1. A global algorithm was chosen to subtract the background. Using both the C-fragment band of the pre-made C9i3X-7C samples and the 20.5 kDa band of biotinylated protein marker, a linear range of densities for the blotting and detection system was predetermined for the c9-tagged C-fragment band of TRH−R1. Any sample would be neglected if the density of the C-fragment band exceeded the linear range. The quantification of the percentage of disulfide cross-linking was calculated using the formula

$$\text{Percentage of disulfide cross-linking} = \frac{DCF_{reducing} - DCF_{nonreducing}}{DCF_{reducing}} \times 100\%$$

where $DCF_{reducing}$ is the density of the C-fragment band under reducing condition, and $DCF_{nonreducing}$ is the density of the same band under nonreducing condition.

Molecular Modeling. The simulations were carried out with the all-atom PARAM 22 force field (*38*) of CHARMM27 (*39*), which includes phospholipids (*40*) and TIP3P water potentials (*41*). The nonbonded list was generated using an atom-based cutoff of 12 Å. Constant dielectric of 1 was used for electrostatic interaction. Both the electrostatic and van der Waals interactions were smoothly switched from 8 to 11 Å. The switching function was applied only to the force and the energy was evaluated as the integral of the force. The SHAKE (*42*) algorithm was used to fix the length of all bonds involving hydrogen atoms. A time step of 0.002 ps was used. The simulations utilized the parallel version of CHARMM and generated approximately 0.25 ns trajectory per day on 16 Athlon processors of the NIH Biowulf/Lobos3 cluster with Myrinet connections.

Initial TRH−R1 Structure. The initial TRH−R1 model was previously constructed by Colson and colleagues (*30*, *43*). In this model, N-terminal residues 1−29, ICL3 residues 226−260, C-terminal residues 336−393 were removed. As it became apparent that TMH1 was not long enough to span the lipid bilayer, we expanded the range of TMH1 to include residues 26−52. The new TMH1 structure was generated as described in (*44*). The TRH−R1 model with the modified TMH1 was minimized using the CHARMM program.

Construction of Unoccupied TRH−R1/Lipid/Water System. The initial receptor and hydrated lipid bilayer system was constructed using a procedure that was developed by Woolf, Roux and colleagues (*45*−*47*). In brief, TRH−R1 was positioned so that the axis of the helical bundle was oriented perpendicular to the membrane-solution interface in a vertical position that left the extracellular and intracellular loops in contact with the bulk water and the transmembrane helices in contact with the lipid acyl chains. The membrane normal was oriented along the *z*-axis, and the center of the bilayer was set at $z = 0$ Å. Dimyristoylphosphatidylcholine (DMPC) molecules were selected randomly from a preequilibrated and prehydrated conformer library (*45*, *48*) and placed around the receptor. Initial positioning of DMPC, removal of bad contacts between individual molecules (lipids, receptor and water) and construction of the remaining bulk water were achieved as described in previous studies (*45*−*47*). The entire system was built in a hexagonal unit cell. The dimensions of the hexagonal unit cell were set to a=b=62 Å and c =

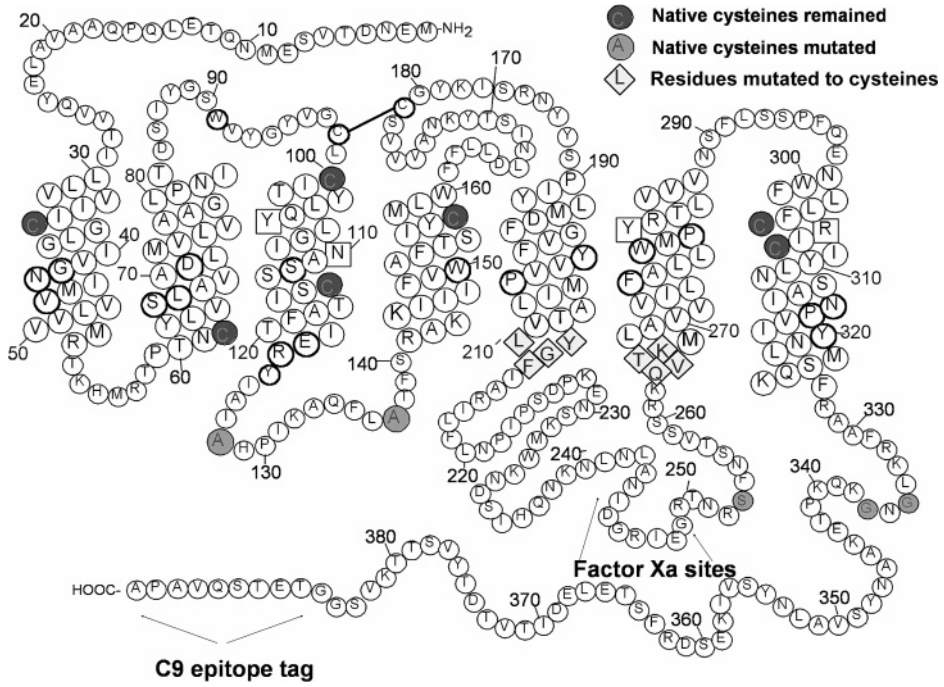

FIGURE 1: 2-D topology of mTRH−R1 construct: C9i3X-7C. C9 epitope tag is linked to Ser-383 of C-terminus with two glycine residues. Two factor Xa sites (IDGRIEGR) are inserted between Ala-249 and Thr-250. Five endogenous cysteines (light shade) were substituted: Cys-335 and Cys-337 of C-terminus to Gly; Cys-128 and Cys-137 of ICL2 to Ala; Cys-253 of ICL3 to Ser. Seven endogenous free cysteines remain in the TMHs (dark shade): Cys-36 (TMH1), Cys-62(TMH2), Cys-100 and Cys-114 (TMH3), Cys-157 (TMH4), Cys-305 and Cys-308 (TMH7). The residues in squares constitute the transmembrane binding pocket for TRH.

92 Å, which led to 23 DMPC molecules per layer and ∼ 4400 water molecules. This setup warranted about three DMPC molecules between the receptor and any of its six mirror images. The final system consisted of ∼23000 atoms. The temperature of the system was set to 310 K, above the gel-liquid-phase transition temperature of DMPC (296.9 K) (*49*). Periodic boundary conditions were applied during the simulations. A multistep procedure to relax the lipid bilayer and water was also performed following the procedure of Woolf and Roux. An additional equilibration run of 800 ps was carried out in the microcanonical ensemble (NVE). Constant pressure simulation would be more desirable; however, at this stage the NVE ensemble was chosen to avoid possible difficulties due to the significant pressure anisotropy and possible inhomogeneity of the simulation cell.

Construction of TRH-Occupied TRH−R1/DMPC/Water System. The system of TRH-occupied TRHR was constructed from the unoccupied system. A two-stage restrained molecular dynamics was used to place TRH in the transmembrane binding pocket. In the unoccupied model, the side chain of Ile109 was approximately in the middle of the crevice in which TRH would be positioned in the occupied model (*44*, *50*). Therefore, initially the δ-carbon atom of Ile109 was fixed, and the TRH molecule was manually placed in the extracellular space. A nuclear overhauser enhancement (NOE) distance restraint as encoded in CHARMM (K_{max} = 50 kJ/mol/Å^2, K_{min} = 10 kJ/mol/Å^2, r_{max} = 36.5 Å, r_{min} = 2 Å) was applied between the pyroGlu group of TRH and the fixed carbon of Ile109 during the first 20 ps of molecular dynamics simulation (NVT, T=310 K). For every subseqeunt 20 ps of simulation, r_{max} was reduced by 1 Å. This simulation progressively pulled the TRH into the binding pocket. After 600 ps of simulation, the restraint on the δ-carbon atom of Ile109 and the NOE restraint were released. In the second stage, NOE restraints corresponding to identified TRH binding pocket interactions were applied and gradually the r_{max} was reduced to 3 Å during the dynamics simulation. The restraints (K_{max} = 50 kJ/mol/Å^2, K_{min} = 10 kJ/mol/Å^2) included: 1) the ring carbonyl group of pyroGlu of TRH to the hydroxyl group of Tyr-106; 2) the ring N−H of pyroGlu of TRH to the side chain carbonyl of Asn-110; 3) the terminal carboxamide of ProNH2 of TRH to the guanidinium group of Arg-306; 4) the side chain ring of His of TRH to side chain ring of Tyr-282. The second stage simulation was run for 2 ns. At the end of the simulation, TRH and the binding pocket were similar to the structure that was constructed previously (*44*, *50*).

Generating Initial Conformations Based on Disulfide Cross-Linking Experiments. The disulfide cross-linking data of the four double-cysteine mutants were used to further refine the initial conformations. NOE restraints were applied to the distances between α carbons of Gln-263/Gly-212, Gln-263/Tyr-211, Thr-265/Gly-212 and Thr-265/Tyr-211. The center of the distance restraints were (10.2 Å, 11.0 Å, 13.8 Å, 13.8 Å) and (18.5 Å, 17.5 Å, 13.1 Å, 13.1 Å) for unoccupied or TRH-occupied model, respectively. The widths of the NOE restraints were 2 Å. The force constants (K_{max} and K_{min}) were 5 kJ/mol/ Å^2 for 500 ps MD simulations, and then reduced to 1 kJ/mol/ Å^2 for additional 500 ps MD simulations. Although the values chosen for distance restraints were rather arbitrary, they did reflect the experimental results. We expected that subsequent MD simulations without any restraint would generate trajectories that were not strongly dependent on the exact values. The restraints corresponding to TRH binding pocket interactions were kept on throughout this 1 ns simulation for the TRH-occupied model.

Molecular Dynamic Simulation without Restraint. To examine the correlation between the models and experiments, unrestrained molecular dynamics simulations of 5 ns were performed on each model using NVT ensembles at 310 K. These simulations would allow us to find stable conformations for each model, which would help evaluate the refined models. Five ns is relatively long compared to similar studies reported previously (*51*, *52*) but are not long compared to the time needed to change rhodopsin conformation (see Discussion). They should, nevertheless, provide good sampling. Structures were saved every 0.5 ps to generate two trajectories of 10000 snapshots each. For each model, the four Cα-Cα distances mentioned above were calculated throughout the 5 ns trajectory. Within the initial 500 ps, the distances changed from the initial value and stabilized progressively. Therefore the first 500 ps were not considered and distance distributions were calculated using the last 4.5 ns of the trajectories.

Modeling of the Four Double-cysteine Mutants. Representative structures of unoccupied and TRH-occupied model (at 2.5 ns) were chosen for *in silico* mutagenesis, to generate the double-cysteine mutation models: Q263C/Y211C, Q263C/G212C, T265C/Y211C and T265C/G212C. The mutations were performed using the software Insight II (Accelrys, San Diego). A 100-step Adopted Basis Newton−Raphson (ABNR) energy minimization was applied to resolve bad contacts caused by the replacement. Further molecular dynamics simulations of these 8 new models were performed to generate 5 ns trajectories for each model. The first 500 ps segment was discarded assuming this was the time for equilibration. Distance distributions of α carbons and sulfur atoms of the cysteine pairs were calculated for the last 4.5 ns trajectories of the eight models.

Data Analysis. All nonlinear regression fits and histograms of distributions were performed using the program Prism (GraphPad). The distances and RMSD (root-mean-square deviation) calculation for the model were performed using the software CHARMM.

RESULTS

Disulfide Cross-Linking of Endogenous TMH Cysteines. C9i3X-7C, in which Cys residues within ICLs were replaced and the highly conserved Cys pair (Cys-98 and Cys-179) that forms a disulfide bond between the first and the second extracellular loops (ECLs) was retained, was constructed. C9i3X-7C contained 7 free endogenous Cys residues (Figure 1). The K_i of TRH binding to C9i3X-7C was indistinguishable (20 ± 7 nM) from TRH−R1 (21 ± 6 nM) (Figure 2A). C9i3X-7c and TRH−R1 exhibited similar signaling properties with the same EC50 of 0.4 ± 0.1 nM (Figure 2B). We determined whether any of the endogenous Cys residues within TMH1−5 could form disulfide bonds with those in TMH6−7. C9i3X-7C solubilized from transfected cells appeared as 2 bands on SDS−PAGE by Western analysis with 1D4 antibody (Figure 3A). The lower band represents intact monomeric C9i3X-7C while the upper band most likely represented receptor oligomers. The density of the upper band is much lower than that of monomeric receptor. As expected, treatment with factor Xa yielded a single band of ∼20 kDa, which is consistent with the C9-tagged C-fragment (Figure 3B). When the sample was treated with

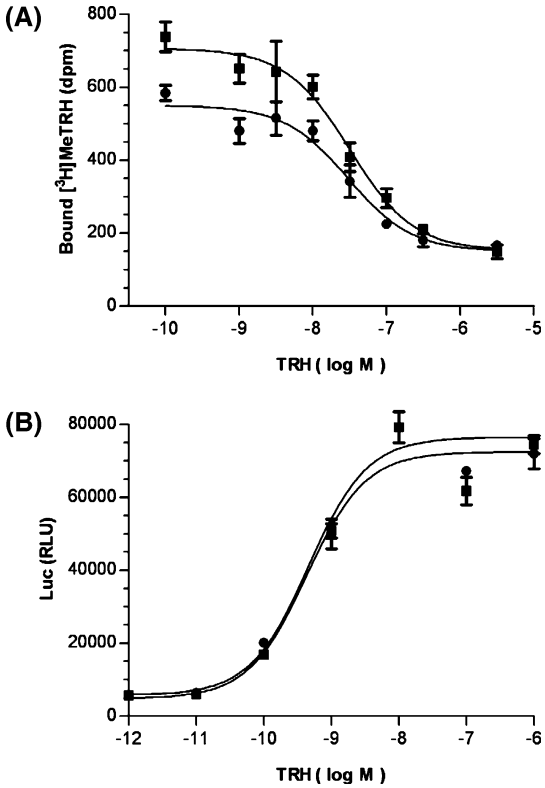

FIGURE 2: The TRH−R1 mutant, C9i3X-7C, has similar pharmacological properties to TRH−R1. (A) Competition binding. The Kis of TRH are 21 ± 6 nM for TRH−R1 (filled squares) and 20 ± 7 nM for C9i3X-7C (filled circles). (B) Signaling. TRH−R1 (filled squares) and C9i3X-7C (filled circles) show low basal activity, similar efficacy and EC50 (0.4 ± 0.1 nM and 0.4 ± 0.1 nM). Results are expressed as mean ± SEM of assays performed in triplicate in a representative experiment.

Cu(II)-phenanthroline, as shown in the two lanes on the left, the density of the C-fragment band was reduced under the nonreducing condition, consistent with disulfide bond formation between endogenous cysteines in TMH1−5 and TMH6−7. However, the band corresponding to the holoreceptor appeared to aggregate under oxidizing conditions and was seen as a smeared band with higher apparent molecular weight. In support of this idea, β-ME reduced a majority of the aggregate to monomeric receptor (Figure 3C). Therefore, disulfide bonds between TMH1−5 and TMH6−7 can be induced. Since we found disulfide bond formation at 5 min (37 ± 6%) that reached an apparent plateau between 5 and 30 min (43 ± 5%) and treatment for 60 min or longer caused receptor degradation, we used cross-linking for 30 min in all subsequent experiments.

To determine which Cys residues cross-linked to Cys-305/308, three mutant receptors, C1 (lacking Cys-100 and -157), C4 (lacking Cys-36 and -157) and C8 (lacking Cys-36 and -100) were studied. Mutants of Cys-62 and Cys-114 were not constructed because our model predicted they were too far apart to cross-link (*25*) and their inability to be involved in cross-linking confirmed because there was no cross-linking in C4 and C8 (Figure 4). The percentage for C1 (36 ± 4%) is similar to that of C9i3X-7C (42 ± 2%). Thus, only Cys-36 (TMH1) can form a disulfide bond with Cys-305/308 (TMH7).

Disulfide Cross-Linking of Engineered Cysteines at the Cytoplasmic Ends of TMH5 and TMH6. To study disulfide

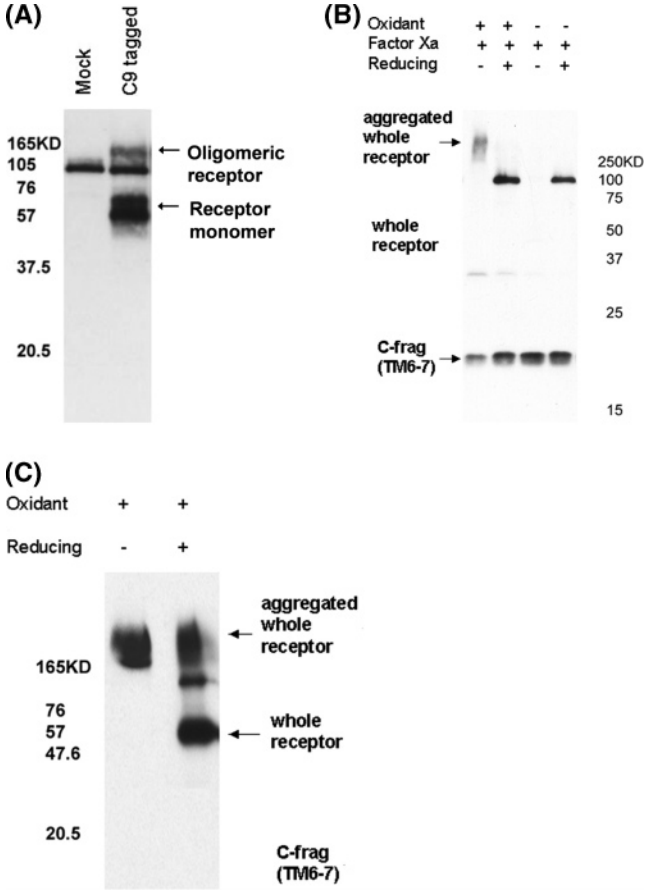

FIGURE 3: Endogenous cysteines in C9i3X-7C form disulfide bonds. (A) C9i3X-7C expression sample (right lane) and mock transfected sample (left lane). A major band corresponding to monomeric receptors (50−65 kDa), and a minor band of oligomeric receptor (> 120 kDa) were specifically detected. The band (~100 kDa) was nonspecific. (B) Endogenous cysteines within TMH1−5 formed disulfide bonds with Cys-305/308 of TMH7. The difference between the densities of C-fragment bands (~20 kDa) between lane 1 and 2 indicated that under the nonreducing condition, a portion of C-fragment was disulfide linked to N-fragment. Lanes 3 and 4 served as a control for oxidation, where there was minimal (<5%) of cross-linking. (C) Reduction of oxidation-induced aggregation of intact receptors.

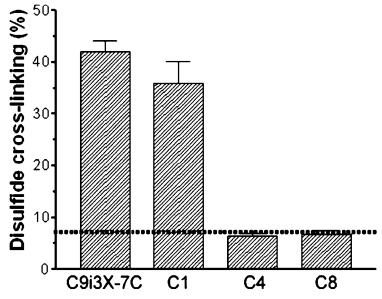

FIGURE 4: Cys-36 (TMH1) cross-links to Cys-305/308 (TMH7). Cross-linking was significant only when Cys-36 was present. C1 lacks Cys-100 and Cys-157. C4 lacks Cys-36 and Cys-157, and C8 lacks Cys-36 and Cys-100. Error bars indicate standard errors. Each number is obtained from three independent experiments. The dotted-line (7%) represents the threshold for disulfide formation.

cross-linking at the cytoplasmic ends of TMH5 and TMH6, C9i3X-3C, in which the only remaining endogenous free Cys residues are Cys-36, Cys-100 and Cys-157, was constructed as the template upon 16 double-Cys mutants were made. In each mutant, one residue of the sequence from Leu-210 to Phe-213 at the cytoplasmic end of TMH5 and another from Gln-263 to Lys-266 at the cytoplasmic end of TMH6 were mutated to Cys. All of these mutant receptors responded maximally to TRH but their potencies for TRH were, in general, lower than those of C9i3X-3C and TRH−R1 (Table 1). The disulfide cross-linking result for four double-cysteine mutants, Q263C/L210C, Q263C/Y211C, Q263C/G212C, and Q263C/F213C in the absence or presence of saturating dose of TRH are shown in Figure 5A. Cys-263 of TMH6 cross-linked more with either Cys-212 or Cys-211 of TMH5 than with Cys-210 or Cys-213, and this cross-linking was inhibited by TRH.

With unoccupied T265C/L210C, T265C/Y211C, T265C/G212C and T265C/F213C there was significant cross-linking whereas with TRH occupancy T265C/Y211C and T265C/G212C showed significant increases in cross-linking from 10 ± 2% to 21 ± 3% and from 10 ± 3% to 20 ± 5%, respectively. In contrast, cross-linking in T265C/L210C and T265C/F213C was minimally increased by TRH from 4 ± 6% and 10 ± 5% to 13 ± 5% and 13 ± 4%, respectively. In summary, Cys265 of TMH6 was unlikely to form a disulfide bond with any of the four cysteines of TMH5 in the absence of TRH but TRH occupancy led to cross-linking in T265C/Y211C and T265C/G212C.

Table 1: The Potencies of TRH (nM) for the Sixteen Double-Cysteine Mutants[a]

TMH5 mutation	TMH6 mutation				
	none	Q263C	V264C	T265C	K266C
none	12 (5)	93 (11)	2200 (700)	74 (13)	62 (22)
L210C	16 (3)	36 (7)	3000 (500)	37 (5)	110 (40)
Y211C	340 (60)	3000 (800)	5000 (1000)	1300 (200)	710 (80)
G212C	140 (30)	1700 (400)	1300 (300)	1300 (300)	70 (20)
F213C	7 (1)	300 (80)	1700 (600)	13 (3)	18 (4)

[a] The data represent the mean (SEM) of triplicate determinations in two independent experiments.

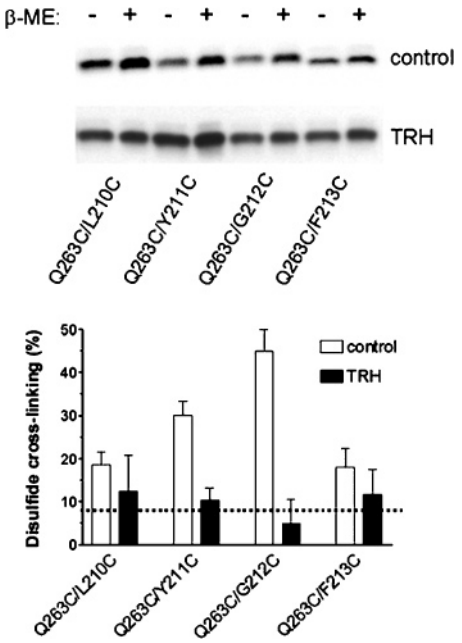

FIGURE 5: Disulfide cross-linking of the double-cysteine mutants. The upper panel is a representative experiment. The lower panel represents quantification over five independent experiments. The dotted-line (7%) represents the threshold for disulfide formation.

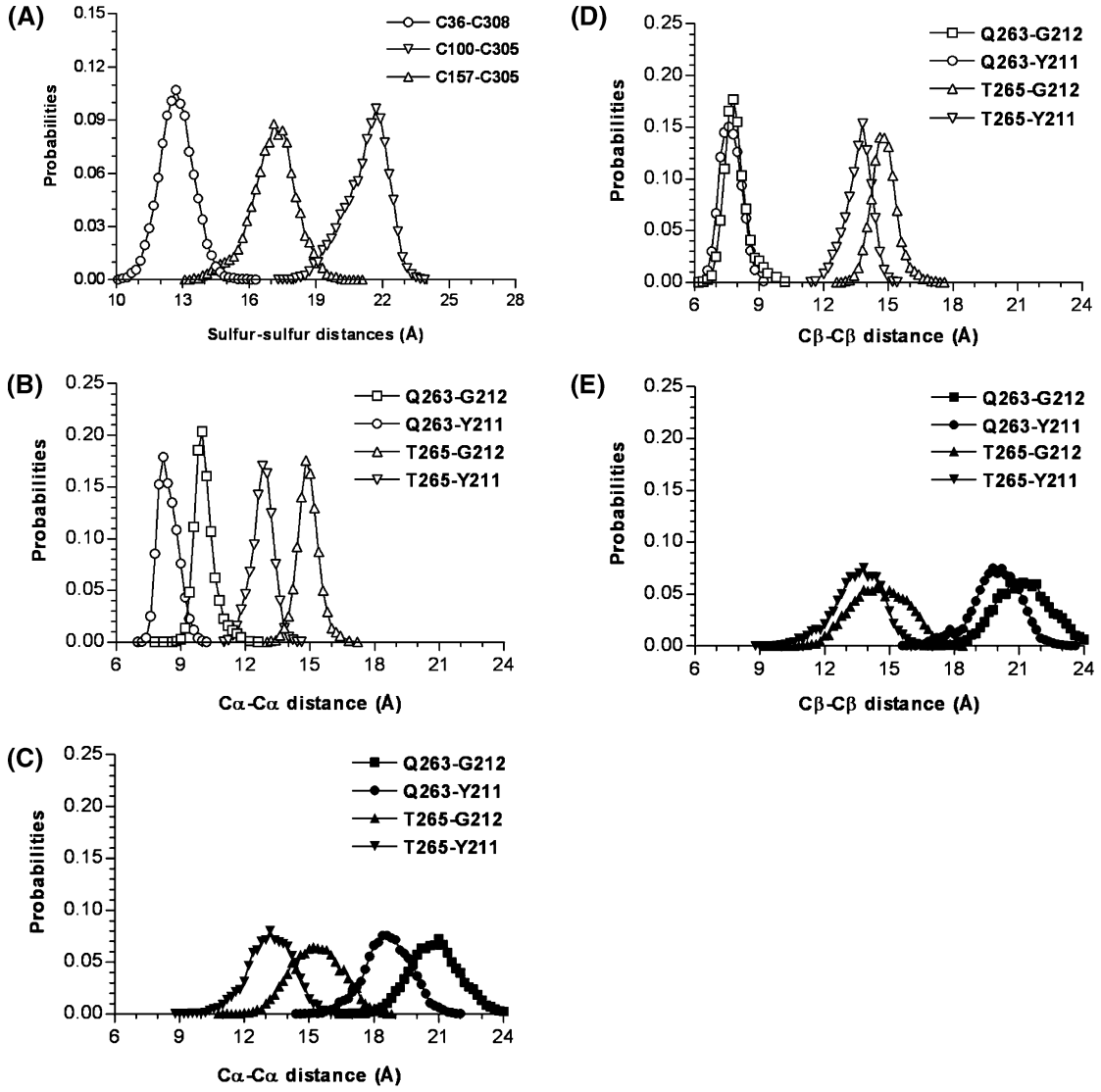

FIGURE 6: TRH−R1 models are consistent with experimental results. The distances between corresponding atom pairs were measured and histograms were calculated with bin site of 0.2 Å, from the 4.5 ns trajectories (9000 structures). (A) Sulfur−sulfur distance distribution of the unoccupied receptor model. (B) Cα-Cα distance distributions of the unoccupied receptors model. (C) Cα-Cα distance distributions of the TRH-occupied receptor model. (D) Cβ-Cβ distance distributions of the unoccupied receptor model. The coordinates of the corresponding hydrogen linked to the alpha carbon of Gly-212 was used as a surrogate. (E) Cβ-Cβ distance distributions of the TRH-occupied receptor model.

For V264C/Y211C, V264C/G212C, and V264C/F213C, cross-linking was not significant in the absence or presence of TRH. For V264C/L210C, cross-linking was low and there was no response to TRH. The last four double-cysteine mutants, K266C/L210C, K266C/Y211C, K266C/G212C, and K266C/F213C, did not exhibit cross-linking in the absence or presence of TRH.

Refinements of TRH−R1 Models. The prediction from our previous TRH−R1 model that TRH induced separation of TMH5 and TMH6 at their cytoplasmic ends (*30*) was consistent with our disulfide cross-linking experiments. However, the hierarchy of Cα-Cα distances of the model was not in agreement with experimental results. The discrepancies might have been because TRH−R1 was simulated with an effective dielectric constant intended to represent the effect of the lipid. The recent development of models of membrane proteins in explicit lipid bilayers (*53*) suggested that our TRH−R1 would be improved by embedding it in a realistic environment of an explicit lipid bilayer and water.

Comparison between the Refined Models and the Disulfide Cross-Linking of Endogenous Cysteines. We compared the distance distributions of the Cys residues in the model, calculated from the sulfur−sulfur distances of Cys-36 to Cys-305/308, Cys-100 to Cys-305/308 and Cys-157 to Cys305/308 (Figure 6A) and the experimental results of disulfide bond formation. The distances indicate that Cys-36 is the most likely residue to form a disulfide bond with Cys-305/308. The combination of the experimental and modeling approaches confirmed the close proximity between Cys-36 (TMH1) and Cys-305/308 (TMH7) of TRH−R1 (*54*).

Comparison of the Models of TRH−R1 and the Disulfide Cross-Linking of the Double-Cysteine Mutants. We calculated the distance distribution of α carbons of the corresponding residue pairs in the TRH−R1 model. Based on a survey of structurally determined proteins, the Cα −Cα distance of two Cys residues that form a disulfide bond is between 3.6 and 6.8 Å (*55*). However, disulfide cross-linking has been demonstrated between Cys residues with α-carbons

15 Å apart in the X-ray structure of the D-galactose chemosensory receptor (*56*). In the same study, the monotonical correlation between the percentages of disulfide cross-linking and the Cα-Cα distances was also established. From the 4.5 ns trajectories of unoccupied and TRH-occupied TRH−R1 models, the distributions of Cα −Cα distances displayed a hierarchy of Cα-Cα distance distributions of Gln-263/Tyr-211 < Gln-263/Gly-212 < Thr-265/Tyr-211 < Thr-265/Gly-212 in the model of the unoccupied receptor (Figure 6B). Disulfide cross-linking indicated a hierarchy of Gln-263/Gly-212 < Gln-263/Tyr-211 < Thr-265/Tyr-211 = Thr-265/Gly-212, which is generally consistent with the model except that the experiment suggested Gly-212, instead of Tyr-211, is closer to TMH6. For the TRH-bound TRH−R1, both experiments and models (Figure 6C) indicated the same hierarchy of the Cα-Cα distance distributions of Thr-265/Tyr-211 < Thr-265/Gly-212 < Gln-263/Tyr-211 < Gln-263/Gly-212.

Cα-Cα distances partly reflect interhelical arrangements that are determined by the backbone structure of the helices. The Cβ-Cβ distances, on the other hand, depend on side chain orientations, which are more relevant to disulfide cross-linking. The Cβ-Cβ distances were calculated for unoccupied (Figure 6D) and TRH-occupied models (Figure 6E), respectively. The coordinates of the hydrogen corresponding to Cβ of Gly-212 were used as a surrogate during the calculation. For the unoccupied model, the notable difference is that the distance distributions of Gln-263/Gly-212 and Gln-263/Tyr-211 are indistinguishable. This indicates that the α carbon of Tyr-211 is closer to TMH6 than that of Gly-212, but Gly-212 is pointed more directly to TMH6 than Tyr-211. The difference between the distance distributions of Thr-265/Gly-212 and Thr-265/Tyr-211 is also smaller, which also fits better with the experiment. For the occupied model, the Cβ-Cβ distance distributions are similar to those of Cα-Cα except for the distance difference between Thr-265/Gly-212 and Gln-263/Tyr-211. This difference also fits the experiments better. It is clear that the Cβ-Cβ distance distributions are more consistent with cross-linking results.

The average Cβ-Cβ distance of Thr-265/Tyr-211 is reduced by 0.8 Å by TRH binding, which is consistent with TRH-induced increase in disulfide cross-linking of Q265C/Y211C. However, the average Cβ-Cβ distance of Thr-265/Gly-212 is increased by 0.9 Å by TRH binding, although the cross-linking is increased. As the disulfide formation is influenced by both the average distance and distance distribution, the wider distribution of Thr-265/Gly-212 in the TRH-occupied model provides a mechanism to interpret the experimental results. In fact, all of the distances demonstrated a wider distribution in the TRH-occupied model. This is consistent with the general idea that activated 7TMRs are more structurally flexible than inactive ones (*57*). Overall, the refined models are more consistent with experimental results than the previous models but still do not correctly predict all aspects of the experiments.

Comparison of the in Silico Double-Cysteine Mutants with the Disulfide Cross-Linking of Double-Cysteine Mutants. To more directly compare the experimental and modeling results, we generated *in silico* 8 unoccupied or TRH-occupied double-cysteine mutants − Q263C/Y211C, Q263C/G212C, T265C/Y211C and T265C/G212C. In general, the distance distributions for the *in silico* mutants (Figure 7A,B) are similar to those for corresponding wild-type models (Figure 6B, C). These findings suggest that the double-cysteine mutations did not cause significant conformational changes at the cytoplasmic ends of TMH5 and TMH6. Notable differences were found in the mutant models of unoccupied Q263C/Y211C. For the Q263C/Y211C model, the unoccupied receptor displays a wider Cα-Cα distance distribution. The significance of these exceptions and their relationship to apparent potencies of TRH for corresponding double-cysteine mutants are not easily interpretable.

The distance distributions of the sulfur atoms of the Cys pairs are shown in Figure 8. TRH occupancy caused the distribution to shift to the right for both Q263C/Y211C and Q263C/G212C models, which correlates well with the experimental results that TRH causes decreases of disulfide cross-linking of these two double-Cys mutants (Figure 8A). Although TRH occupancy does not shift the average sulfur−sulfur distance of T265C/Y212C, it causes a wider distribution (Figure 8B) that is consistent with increases in disulfide bond formation. The sulfur−sulfur distance distributions of T265C/G212C are not in agreement with experimental results, as shown with the TRH-induced right shift of the distribution for the model and apparent increasing in disulfide bond formation in the experiments. This discrepancy has also been revealed in the analysis of Cα-Cα distance distributions of the wild-type model (Figure 6). These results suggest that the actual structure of TRH−R1 with regard to the relative positions of Tyr-211 and Gly-212 are not well represented in the models.

DISCUSSION

In the present study, we used Cys-scanning mutagenesis and disulfide cross-linking to directly probe conformational changes at the cytoplasmic ends of TMH5 and TMH6 during TRH−R1 activation. The TRH−R1 molecular models were refined in explicit lipid bilayers and water solvent with initial restraints derived from experimental results. Relaxation and equilibration of the refined models using 5 ns molecular dynamics simulations resulted in trajectories that were in most aspects in agreement with experimental results as were MD simulations of *in silico* double-Cys mutant models. Disulfide cross-linking approaches have been used previously to study the activation process of rhodopsin (*6, 58*) and m3 muscarinic receptors (*8*). Nevertheless, to our knowledge, this is the first study of 7TMR activation using a combination of disulfide cross-linking and molecular modeling of wild type and mutant receptor models embedded in hydrated lipid bilayers.

Our implementation of disulfide cross-linking was similar to the studies of the m3 muscarinic receptor (*7, 8*). However, several modifications were made to reduce variations in the results. For example, by dividing one factor Xa-digested sample into two aliquots, we eliminated the variations introduced during the solubilization, immunoprecipitation, elution and factor Xa digestion steps that were otherwise unavoidable. Immunoprecipitation and specific elution using C9 peptide before factor Xa digestion increased the purity of the sample. Immobilization of 1D4 antibody eliminated the potential interference of IgG bands. The method was shown to be effective by confirming the close proximity of Cys-36 (TMH1) and Cys-305/308 (TMH7), which is con-

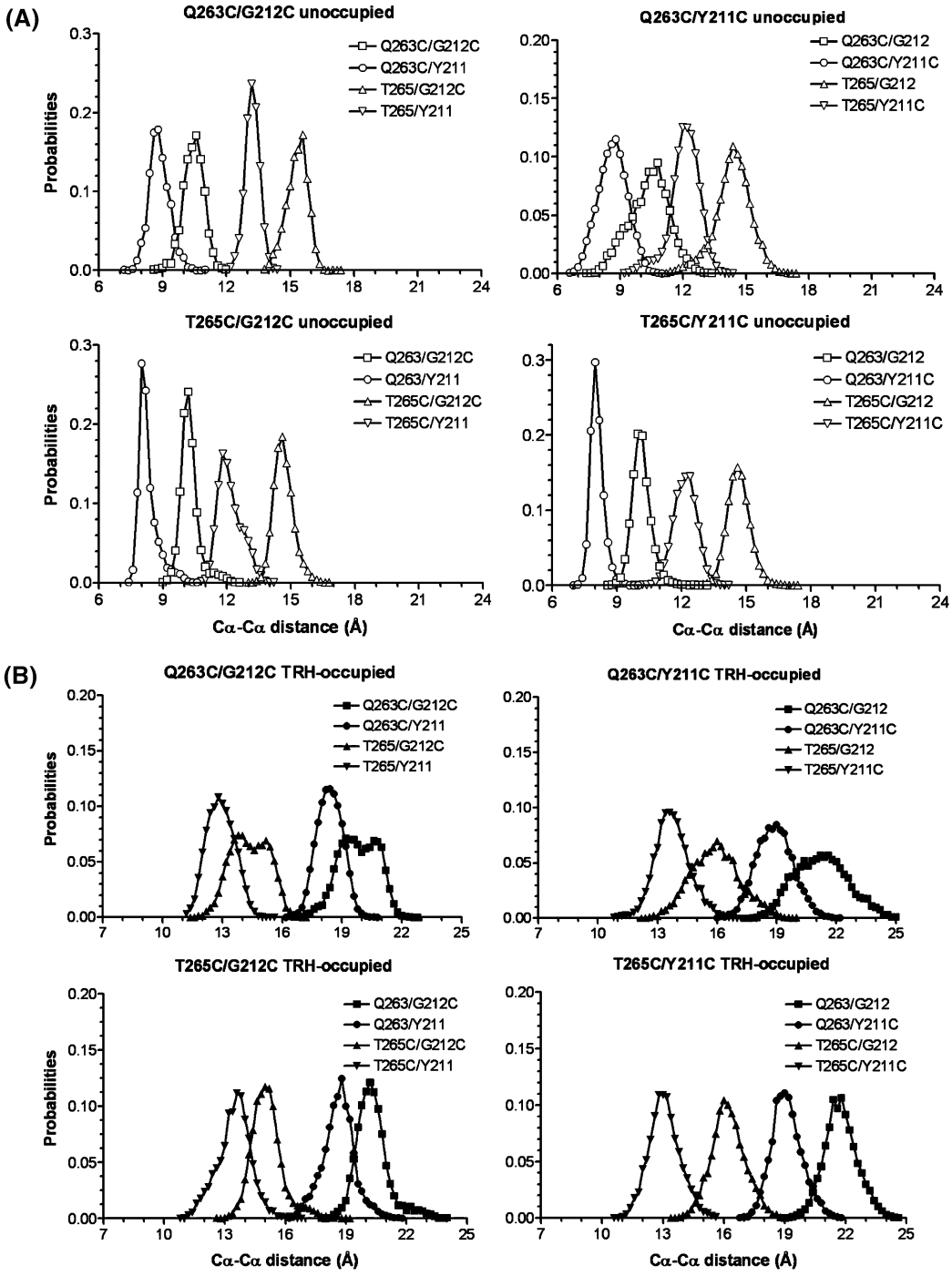

FIGURE 7: *In silico* double-cysteine mutations did not change the conformation of the TRH−R1. Distributions of Cα-Cα distance in Q263C/Y211C, Q263C/G212C, T265C/Y211C and T265C/G212C with or without TRH binding. (A) Cα-Cα distance distributions for four mutant models in the absence of TRH. (B) Cα-Cα distance distributions for four mutant models in the present of TRH.

sistent with predictions from our model and previous experimental results (*31*).

The rate constant of disulfide formation is related to the proximity of the two Cys residues in the protein structure and their dynamics. As reported previously (*59*), the O_2/Cu-phenanthroline oxidative system yields both disulfide bonds and additional sulfhydryl oxidation products that prevent the percentage of disulfide formation from reaching 100%. The percentage of disulfide cross-linking is also monotonically correlated with the rate constant as demonstrated experimentally using the D-galactose chemosensory receptor (*56*). The rate constant, however, is difficult to obtain. We used the percentage of cross-linking as estimates of the rates of formation. Since rate constants for disulfide formation are affected by the collision rate of the two sulfhydryl groups, they depend on both the average distance between the sulfurhydryl groups and the fluctuations of the distance between them. A distance between the sulfhydryl groups could in principle be evaluated by EPR spectroscopy but these have only been performed on one 7TMR, rhodopsin (*58*).

Experiments with 16 double Cys mutant receptors were consistent with the idea that Gln-263 is close to Gly-212 and Tyr-211 in the unoccupied, inactive receptor but that Thr-265 is closer to Tyr-211 and Gly-212 in the TRH-occupied, activated receptor. Moreover, the highest cross-

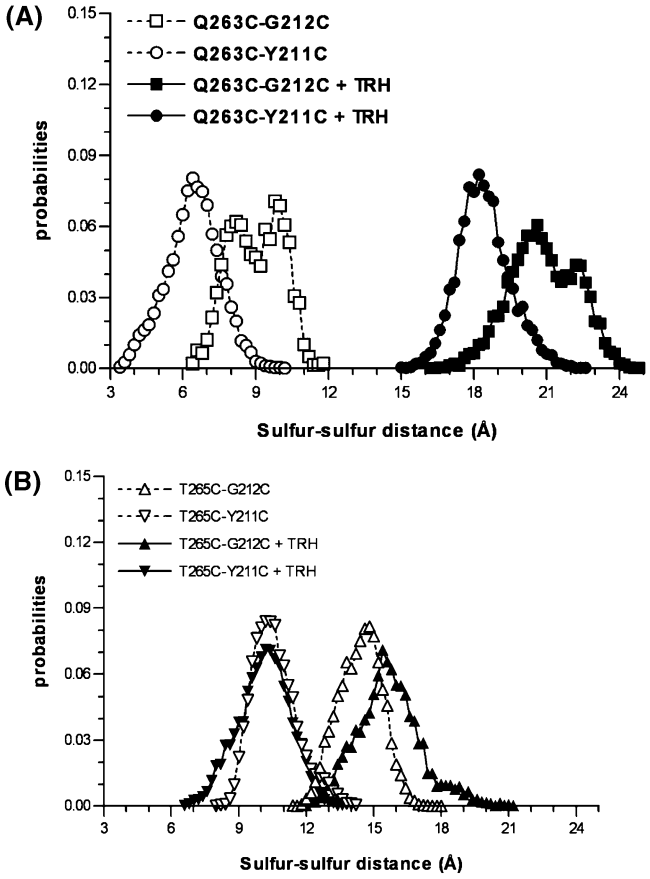

FIGURE 8: *In silico* double-cysteine models were consistent with experimental results. Distributions of sulfur−sulfur distances in (A) Q263C/Y211C or Q263C/G212C in the absence or in the present of TRH, and in (B) T265C/Y211C or T265C/G212C in the absence or in the present of TRH.

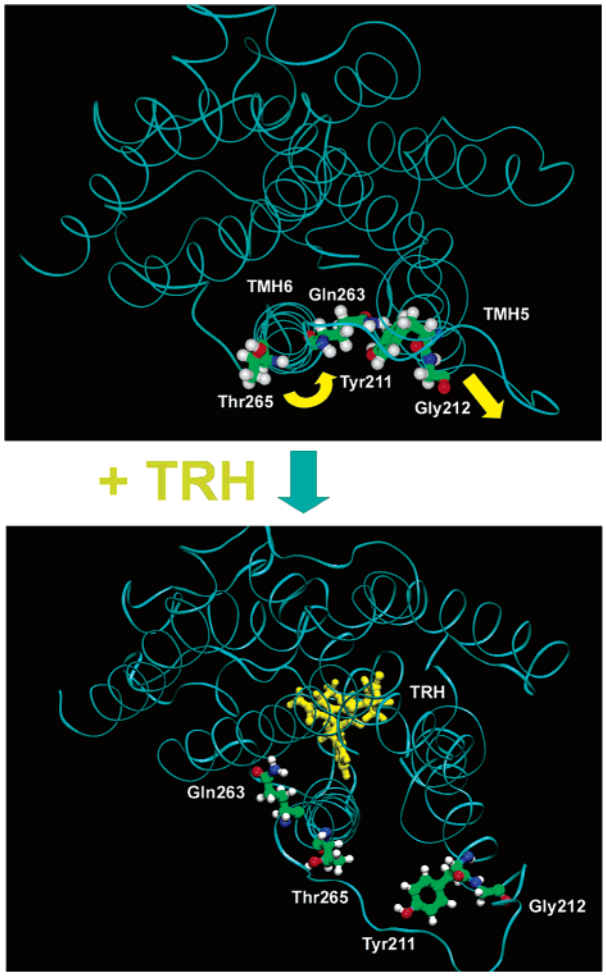

FIGURE 9: The activation model of the TRH−R1 receptor. The upper panel shows a representative structure of inactive unoccupied TRH−R1, while the lower panel shows that of activated TRH-occupied TRH−R1. These are viewed from the cytoplasm. The backbones of transmembrane helices are in cyan. TRH, located in the transmembrane binding pocket, is in yellow. Tyr-211 and Gly-212 of TMH5, and Gln-263 and Thr-265 of TMH6 are represented in ball-and-stick. The lipid bilayer and water molecules are not shown. The TRH-induced conformational changes at the cytoplasmic ends of TMH5 and TMH6 are indicated with yellow arrows.

linking in the absence of TRH (45 ± 5% for Q263C/G212C) is significantly higher than the highest cross-linking in the presence of TRH (21 ± 3% for T265C/Y211C) that is consistent with the hypothesis that TRH induces a separation between the cytoplasmic ends of TMH5 and TMH6 (*30*). Molecular dynamic simulations of the TRH−R1 models provided better intepretations of the experiments with both static and dynamic information of the distances between the corresponding residue pairs. It is noteworthy that several previous studies suggested that the complete transmembrane helical rearrangement that is involved in receptor activation could not occur within 10 ns of simulations of 7TMR-bilayer system (*52*, *60*). We acknowledge the relatively short interval of our simulations but suggest that our findings likely represent intermediates in the activation process. We did, however, use the experimental data to force the transition of the TRH−R1 model from inactive to active states and thereby generate a model closer to the final activated state. Nevertheless, longer simulations dependent on progress in computer technology will be needed for more realistic models.

Our findings are consistent with the following conformational changes in the TMH5−ICL3-TMH6 region induced upon TRH binding: 1) a counterclockwise rotation of TMH6 (viewed from the cytoplasmic side); 2) a tilting of TMH5 away from TMH6; and 3) the combination of the relative rotation and separation of the cytoplasmic ends of TMH5 and TMH6 make key residues, such as Arg 261 and Lys262 (6.30 and 6.31 (*61*)), more accessible for G protein coupling (Figure 9). It has been suggested that Lys-248 (6.31) of rhodopsin (equivalent to Lys262 of TRH−R1) interacts with Asp-310 of the alpha subunit of transducin during rhodopsin activation (28). The residues 218−225 in the TMH5−ICL3 region of TRH−R1 have been shown to be involved in Gq coupling as well (*22*, *29*), and could become more accessible by separating TMH5 and TMH6.

A number of EPR and cross-linking studies focused on the relative movement of the cytoplasmic ends of TMH3 and TMH6 upon activation of rhodopsin (*2*−*4*, *9*, *10*), β2-adrenergic receptor (*15*), m1 muscarinic receptor (*11*), and parathyroid hormone receptor (*10*). We have not studied changes in TMH3 relative to TMH6 in TRH−R1.

A number of recent studies have demonstrated the existence of oligomerization of 7TMRs. Oligomerization, specifically dimerization, has been suggested to be necessary, in certain cases, for interaction with G proteins, endocytosis or altering ligand pharmacology (see (*62*) and references therein). A minor fraction of TRH receptors have been shown to form oligomers (*63*, *64*). Because the majority of TRH−

R1 appear to be present as monomers on the cell surface, oligomerization would not complicate the general conclusions of our study.

Our conclusions regarding the movements of TMH5 and TMH6 in TRH−R1 are different from conclusions reached in previous studies of rhodopsin and several other 7TMRs. For example, EPR (*2*, *65*) suggested that the cytoplasmic end of TMH6 of rhodopsin undergoes a clockwise rotation (cytoplasmic view) following activation. This intepretation was consistent with a de novo model of active forms of rhodopsin built upon these experimental findings (*66*). A fluoresence spectroscopy study of β2-adrenergic receptor activation suggested a clockwise rotation of TMH6 and/or a tilting of the cytoplasmic end of TMH6 toward TMH5 (*15*, *67*). A cross-linking study of the M3 muscarinic receptor suggested that the cytoplasmic ends of TMH5 and TMH6 moved closer during activation (*8*). We cannot explain the different findings in these studies of other 7TMRs, however, it is not certain that all 7TMRs undergo similar conformational changes during activation. Future studies with TRH−R1 and other 7TMRs will be necessary to shed light on this question.

In conclusion, the results of our experiments and computer simulations provide strong evidence that TRH binding induces a separation of the cytoplasmic ends of TMH5 and TMH6 of TRH−R1, and a counterclockwise rotation of TMH6. Furthermore, the computer modeling suggests that these movements are directly linked to G protein coupling as the rotation of TMH6 and the tilting away of TMH5 "opens" up ICL3 and increases the surface accessible area at the juxtamembrane regions of ICL3 leading to exposure of other domains of the TRH−R1 cytoplasmic face. This hypothesis is consistent with the general mechanism proposed for 7TMR activation based on structural studies of rhodopsin in which the movement or rotation of TMH6 away from TMH2, 3 and 5 "opens" the site on the rhodopsin cytoplasmic surface that interacts with transducin (*58*, *68*).

ACKNOWLEDGMENT

We thank Drs. Sharon Worthington, Richard Venable, and Anny-Odile Colson for insightful discussions of the molecular modeling. 1D4 antibody was supplied by theNational Cell Culture Center (Mineapolis, MN). This study utilized the high-performance computational capabilities of the Biowulf PC/Linux cluster at the National Institutes of Health, Bethesda, MD (http://biowulf.nih.gov).

REFERENCES

1. Palczewski, K., Kumasaka, T., Hori, T., Behnke, C. A., Motoshima, H., Fox, B. A., Le Trong, I., Teller, D. C., Okada, T., Stenkamp, R. E., Yamamoto, M., and Miyano, M. (2000) Crystal structure of rhodopsin: A G protein-coupled receptor, *Science 289*, 739−745.
2. Farrens, D. L., Altenbach, C., Yang, K., Hubbell, W. L., and Khorana, H. G. (1996) Requirement of rigid-body motion of transmembrane helices for light activation of rhodopsin, *Science 274*, 768−770.
3. Yang, K., Farrens, D. L., Altenbach, C., Farahbakhsh, Z. T., Hubbell, W. L., and Khorana, H. G. (1996) Structure and function in rhodopsin. Cysteines 65 and 316 are in proximity in a rhodopsin mutant as indicated by disulfide formation and interactions between attached spin labels, *Biochemistry 35*, 14040−14046.
4. Kim, J. M., Altenbach, C., Thurmond, R. L., Khorana, H. G., and Hubbell, W. L. (1997) Structure and function in rhodopsin: rhodopsin mutants with a neutral amino acid at E134 have a partially activated conformation in the dark state, *Proc. Natl. Acad. Sci. U.S.A. 94*, 14273−14278.
5. Struthers, M., Yu, H., Kono, M., and Oprian, D. D. (1999) Tertiary interactions between the fifth and sixth transmembrane segments of rhodopsin, *Biochemistry 38*, 6597−6603.
6. Yu, H., and Oprian, D. D. (1999) Tertiary interactions between transmembrane segments 3 and 5 near the cytoplasmic side of rhodopsin, *Biochemistry 38*, 12033−12040.
7. Zeng, F. Y., Hopp, A., Soldner, A., and Wess, J. (1999) Use of a disulfide cross-linking strategy to study muscarinic receptor structure and mechanisms of activation, *J. Biol. Chem. 274*, 16629−16640.
8. Ward, S. D., Hamdan, F. F., Bloodworth, L. M., and Wess, J. (2002) Conformational changes that occur during M3 muscarinic acetylcholine receptor activation probed by the use of an in situ disulfide cross-linking strategy, *J. Biol. Chem. 277*, 2247−2257.
9. Sheikh, S. P., Zvyaga, T. A., Lichtarge, O., Sakmar, T. P., and Bourne, H. R. (1996) Rhodopsin activation blocked by metal-ion-binding sites linking transmembrane helices C and F, *Nature 383*, 347−350.
10. Sheikh, S. P., Vilardarga, J. P., Baranski, T. J., Lichtarge, O., Iiri, T., Meng, E. C., Nissenson, R. A., and Bourne, H. R. (1999) Similar structures and shared switch mechanisms of the beta2-adrenoceptor and the parathyroid hormone receptor. Zn(II) bridges between helices III and VI block activation, *J. Biol. Chem. 274*, 17033−17041.
11. Lu, Z. L., and Hulme, E. C. (2000) A network of conserved intramolecular contacts defines the off-state of the transmembrane switch mechanism in a seven-transmembrane receptor, *J. Biol. Chem. 275*, 5682−5686.
12. Javitch, J. A., Fu, D., Liapakis, G., and Chen, J. (1997) Constitutive activation of the beta2 adrenergic receptor alters the orientation of its sixth membrane-spanning segment, *J. Biol. Chem. 272*, 18546−18549.
13. Gether, U., Lin, S., and Kobilka, B. K. (1995) Fluorescent labeling of purified beta 2 adrenergic receptor. Evidence for ligand-specific conformational changes, *J. Biol. Chem. 270*, 28268−28275.
14. Gether, U., Ballesteros, J. A., Seifert, R., Sanders-Bush, E., Weinstein, H., and Kobilka, B. K. (1997) Structural instability of a constitutively active G protein-coupled receptor. Agonist-independent activation due to conformational flexibility, *J. Biol. Chem. 272*, 2587−2590.
15. Gether, U., Lin, S., Ghanouni, P., Ballesteros, J. A., Weinstein, H., and Kobilka, B. K. (1997) Agonists induce conformational changes in transmembrane domains III and VI of the beta2 adrenoceptor, *EMBO J. 16*, 6737−6747.
16. Strader, C. D., Fong, T. M., Tota, M. R., Underwood, D., and Dixon, R. A. (1994) Structure and function of G protein-coupled receptors, *Annu. Rev. Biochem. 63*, 101−132.
17. Bluml, K., Mutschler, E., and Wess, J. (1994) Identification of an intracellular tyrosine residue critical for muscarinic receptor-mediated stimulation of phosphatidylinositol hydrolysis, *J. Biol. Chem. 269*, 402−405.
18. Bluml, K., Mutschler, E., and Wess, J. (1994) Functional role of a cytoplasmic aromatic amino acid in muscarinic receptor-mediated activation of phospholipase C, *J. Biol. Chem. 269*, 11537−11541.
19. Burstein, E. S., Spalding, T. A., Hill-Eubanks, D., and Brann, M. R. (1995) Structure−function of muscarinic receptor coupling to G proteins. Random saturation mutagenesis identifies a critical determinant of receptor affinity for G proteins, *J. Biol. Chem. 270*, 3141−3146.
20. Hill-Eubanks, D., Burstein, E. S., Spalding, T. A., Brauner-Osborne, H., and Brann, M. R. (1996) Structure of a G-protein-coupling domain of a muscarinic receptor predicted by random saturation mutagenesis, *J. Biol. Chem. 271*, 3058−3065.
21. Burstein, E. S., Spalding, T. A., and Brann, M. R. (1996) Amino acid side chains that define muscarinic receptor/G-protein coupling. Studies of the third intracellular loop, *J. Biol. Chem. 271*, 2882−2885.
22. Buck, F., Wang, W., Harder, S., Brathwaite, C., Bruhn, T. O., and Gershengorn, M. C. (2000) Juxtamembrane regions in the third intracellular loop of the thyrotropin-releasing hormone receptor type 1 are important for coupling to Gq, *Endocrinology 141*, 3717−3722.
23. Liu, J., Conklin, B. R., Blin, N., Yun, J., and Wess, J. (1995) Identification of a receptor/G-protein contact site critical for signaling specificity and G-protein activation, *Proc. Natl. Acad. Sci. U.S.A. 92*, 11642−11646.

24. Liu, J., Blin, N., Conklin, B. R., and Wess, J. (1996) Molecular mechanisms involved in muscarinic acetylcholine receptor-mediated G protein activation studied by insertion mutagenesis, *J. Biol. Chem. 271*, 6172−6178.
25. Taylor, J. M., Jacob-Mosier, G. G., Lawton, R. G., Remmers, A. E., and Neubig, R. R. (1994) Binding of an alpha 2 adrenergic receptor third intracellular loop peptide to G beta and the amino terminus of G alpha, *J. Biol. Chem. 269*, 27618−27624.
26. Taylor, J. M., Jacob-Mosier, G. G., Lawton, R. G., VanDort, M., and Neubig, R. R. (1996) Receptor and membrane interaction sites on Gbeta. A receptor-derived peptide binds to the carboxyl terminus, *J. Biol. Chem. 271*, 3336−3339.
27. Phillips, W. J., and Cerione, R. A. (1992) Rhodopsin/transducin interactions. I. Characterization of the binding of the transducin-beta gamma subunit complex to rhodopsin using fluorescence spectroscopy, *J. Biol. Chem. 267*, 17032−17039.
28. Phillips, W. J., and Cerione, R. A. (1994) A C-terminal peptide of bovine rhodopsin binds to the transducin alpha-subunit and facilitates its activation, *Biochem. J. 299* (Pt 2), 351−357.
29. Nussenzveig, D. R., Heinflink, M., and Gershengorn, M. C. (1993) Decreased levels of internalized thyrotropin-releasing hormone receptors after uncoupling from guanine nucleotide-binding protein and phospholipase-C, *Mol. Endocrinol. 7*, 1105−1111.
30. Colson, A. O., Perlman, J. H., Jinsi-Parimoo, A., Nussenzveig, D. R., Osman, R., and Gershengorn, M. C. (1998) A hydrophobic cluster between transmembrane helices 5 and 6 constrains the thyrotropin-releasing hormone receptor in an inactive conformation, *Mol. Pharmacol. 54*, 968−978.
31. Gershengorn, M. C., and Osman, R. (2001) Minireview: Insights into G protein-coupled receptor function using molecular models, *Endocrinology 142*, 2−10.
32. Falke, J. J., and Koshland, D. E., Jr. (1987) Global flexibility in a sensory receptor: a site-directed cross-linking approach, *Science 237*, 1596−1600.
33. Lee, G. F., Burrows, G. G., Lebert, M. R., Dutton, D. P., and Hazelbauer, G. L. (1994) Deducing the organization of a transmembrane domain by disulfide cross-linking. The bacterial chemoreceptor Trg, *J. Biol. Chem. 269*, 29920−29927.
34. Wu, J., and Kaback, H. R. (1996) A general method for determining helix packing in membrane proteins in situ: helices I and II are close to helix VII in the lactose permease of *Escherichia coli*, *Proc. Natl. Acad. Sci. U.S.A. 93*, 14498−14502.
35. Nussenzveig, D. R., Matos, M. D., and Thaw, C. N. (1998) Human calcitonin receptor is directly targeted to and retained in the basolateral surface of MDCK cells, *Am. J. Physiol. 275*, C1264−1276.
36. Robbins, A. K., and Horlick, R. A. (1998) Macrophage scavenger receptor confers an adherent phenotype to cells in culture, *Biotechniques 25*, 240−244.
37. Perlman, J. H., Nussenzveig, D. R., Osman, R., and Gershengorn, M. C. (1992) Thyrotropin-releasing hormone binding to the mouse pituitary receptor does not involve ionic interactions. A model for neutral peptide binding to G protein-coupled receptors, *J. Biol. Chem. 267*, 24413−24417.
38. Mackerell, A. D. J., Bashford, D., Bellot, M., Dunbrack, R. L., Jr., Evanseck, J. D., Field, M. J., Fischer, S., Gao, J., Guo, H., Ha, S., Joseph-McCarthy, D., Kuchnir, L., Kuczera, K., Lau, F. T. K., Mattos, C., Michnick, S., Ngo, T., Nguyen, D. T., Prodhom, B., Reiher, W. E., III, Roux, B., Schlenkrich, M., Smith, J. C., Stote, R., Straub, J., Watanabe, M., Wiorkiewicz-Kuczera, J., Yin, D., and Karplus, M. (1998) All-atom emperical potential for molecular modeling and dynamics studies of proteins, *J. Phys. Chem. B 102*, 3586−3616.
39. Brooks, B. R., Bruccoleri, R. E., Olafson, B. D., Statea, D. J., Swaminathan, S., and Karplus, M. (1983) CHARMM: A Program for Macromolecular Engergy, Minimization, and Dynamics Calculations, *J. Comput. Chem. 4*, 187−217.
40. Schlenkrich, M. J., Brickmann, J., Mackerell, A. D. J., and Karplus, M. (1996) in *Biological Membranes. A Molecular Perspective from Computation and Experiment* (Roux, B., Ed.) pp 31−81, Birkhauser, Boston.
41. Jorgensen, W. L., Chandrasekhar, J., Madura, J. D., Impey, R. W., and Klein, M. L. (1983) Comparison of simple potential functions for simulating liquid water, *J. Chem. Phys. 79*, 926−935.
42. Ryckaert, J. P., Ciccotti, G., and Berendsen, J. (1977) Numerical integration of the Cartesian equation of motion of a system with constraints: molecular dynamics of *n*-alkanes, *J. Comput. Phys. 23*, 327−341.
43. Colson, A. O., Perlman, J. H., Smolyar, A., Gershengorn, M. C., and Osman, R. (1998) Static and dynamic roles of extracellular loops in G-protein-coupled receptors: a mechanism for sequential binding of thyrotropin-releasing hormone to its receptor, *Biophys. J. 74*, 1087−1100.
44. Perlman, J. H., Laakkonen, L. J., Guarnieri, F., Osman, R., and Gershengorn, M. C. (1996) A refined model of the thyrotropin-releasing hormone (TRH) receptor binding pocket. Experimental analysis and energy minimization of the complex between TRH and TRH receptor, *Biochemistry 35*, 7643−7650.
45. Woolf, T. B., and Roux, B. (1994) Molecular dynamics simulation of the gramicidin channel in a phospholipid bilayer, *Proc. Natl. Acad. Sci. U.S.A. 91*, 11631−11635.
46. Woolf, T. B., and Roux, B. (1996) Structure, energetics, and dynamics of lipid−protein interactions: A molecular dynamics study of the gramicidin A channel in a DMPC bilayer, *Proteins 24*, 92−114.
47. Berneche, S., Nina, M., and Roux, B. (1998) Molecular dynamics simulation of melittin in a dimyristoylphosphatidylcholine bilayer membrane, *Biophys. J. 75*, 1603−1618.
48. Venable, R. M., Zhang, Y., Hardy, B. J., and Pastor, R. W. (1993) Molecular dynamics simulations of a lipid bilayer and of hexadecane: an investigation of membrane fluidity, *Science 262*, 223−226.
49. Tanaka, K., Manning, P. A., Lau, V. K., and Yu, H. (1999) Lipid Lateral Diffusion in Dilauroylphosphatidylcholine/Cholesterol Mixed Monolayers at the Air/Water Interface, *Langmuir 15*, 600−606.
50. Laakkonen, L. J., Guarnieri, F., Perlman, J. H., Gershengorn, M. C., and Osman, R. (1996) A refined model of the thyrotropin-releasing hormone (TRH) receptor binding pocket. Novel mixed mode Monte Carlo/stochastic dynamics simulations of the complex between TRH and TRH receptor, *Biochemistry 35*, 7651−7663.
51. Choi, G., Landin, J., Galan, J. F., Birge, R. R., Albert, A. D., and Yeagle, P. L. (2002) Structural studies of metarhodopsin II, the activated form of the G-protein coupled receptor, rhodopsin, *Biochemistry 41*, 7318−7324.
52. Saam, J., Tajkhorshid, E., Hayashi, S., and Schulten, K. (2002) Molecular dynamics investigation of primary photoinduced events in the activation of rhodopsin, *Biophys. J. 83*, 3097−3112.
53. Berneche, S., and Roux, B. (2001) Energetics of ion conduction through the K+ channel, *Nature 414*, 73−77.
54. Perlman, J. H., Colson, A. O., Wang, W., Bence, K., Osman, R., and Gershengorn, M. C. (1997) Interactions between conserved residues in transmembrane helices 1, 2, and 7 of the thyrotropin-releasing hormone receptor, *J. Biol. Chem. 272*, 11937−11942.
55. Meng, E. C., and Bourne, H. R. (2001) Receptor activation: what does the rhodopsin structure tell us? *Trends Pharmacol. Sci. 22*, 587−593.
56. Careaga, C. L., and Falke, J. J. (1992) Thermal motions of surface alpha-helices in the D-galactose chemosensory receptor. Detection by disulfide trapping, *J. Mol. Biol. 226*, 1219−1235.
57. Gether, U. (2000) Uncovering molecular mechanisms involved in activation of G protein-coupled receptors, *Endocr. Rev. 21*, 90−113.
58. Cai, K., Klein-Seetharaman, J., Hwa, J., Hubbell, W. L., and Khorana, H. G. (1999) Structure and function in rhodopsin: effects of disulfide cross-links in the cytoplasmic face of rhodopsin on transducin activation and phosphorylation by rhodopsin kinase, *Biochemistry 38*, 12893−12898.
59. Oae, S. (1991) *Organic Sulfur Chemistry: Structure and Mechanism*, CRC Press, Boca Raton, FL.
60. Rohrig, U. F., Guidoni, L., and Rothlisberger, U. (2002) Early steps of the intramolecular signal transduction in rhodopsin explored by molecular dynamics simulations, *Biochemistry 41*, 10799−10809.
61. Ballesteros, J., and Weinstein, H. (1995) Integrated methods for the construction of three-dimensional models and computational probing of structure−function relations in G protein coupled receptors, *Methods Neurosci. 25*, 366−428.
62. Milligan, G. (2004) G protein-coupled receptor dimerization: function and ligand pharmacology, *Mol. Pharmacol. 66*, 1−7.
63. Kroeger, K. M., Hanyaloglu, A. C., Seeber, R. M., Miles, L. E., and Eidne, K. A. (2001) Constitutive and agonist-dependent homooligomerization of the thyrotropin-releasing hormone receptor. Detection in living cells using bioluminescence resonance energy transfer, *J. Biol. Chem. 276*, 12736−12743.

64. Zhu, C. C., Cook, L. B., and Hinkle, P. M. (2002) Dimerization and phosphorylation of thyrotropin-releasing hormone receptors are modulated by agonist stimulation, *J. Biol. Chem. 277*, 28228−28237.

65. Altenbach, C., Klein-Seetharaman, J., Cai, K., Khorana, H. G., and Hubbell, W. L. (2001) Structure and function in rhodopsin: mapping light-dependent changes in distance between residue 316 in helix 8 and residues in the sequence 60−75, covering the cytoplasmic end of helices TM1 and TM2 and their connection loop CL1, *Biochemistry 40*, 15493−15500.

66. Nikiforovich, G. V., and Marshall, G. R. (2003) Three-dimensional model for meta-II rhodopsin, an activated G-protein-coupled receptor, *Biochemistry 42*, 9110−9120.

67. Ghanouni, P., Steenhuis, J. J., Farrens, D. L., and Kobilka, B. K. (2001) Agonist-induced conformational changes in the G-protein-coupling domain of the beta 2 adrenergic receptor, *Proc. Natl. Acad. Sci. U.S.A. 98*, 5997−6002.

68. Okada, T., Ernst, O. P., Palczewski, K., and Hofmann, K. P. (2001) Activation of rhodopsin: new insights from structural and biochemical studies, *Trends Biochem. Sci. 26*, 318−324.

BI048808+